The Journal
of Chemical Physics

ARTICLE

pubs.aip.org/aip/jcp

Decoupling of rotation and translation at the colloidal glass transition

Cite as: J. Chem. Phys. 161, 014507 (2024); doi: 10.1063/5.0205459
Submitted: 26 February 2024 • Accepted: 10 June 2024 •
Published Online: 3 July 2024

John Geiger,[1] **Niklas Grimm,**[2] **Matthias Fuchs,**[2] **and Andreas Zumbusch**[1,a)]

AFFILIATIONS

[1] Fachbereich Chemie, Universität Konstanz, 78457 Konstanz, Germany
[2] Fachbereich Physik, Universität Konstanz, 78457 Konstanz, Germany

[a)] **Author to whom correspondence should be addressed:** andreas.zumbusch@uni-konstanz.de

ABSTRACT

In dense particle systems, the coupling of rotation and translation motion becomes intricate. Here, we report the results of confocal fluorescence microscopy where simultaneous recording of translational and rotational particle trajectories from a bidisperse colloidal dispersion is achieved by spiking the samples with rotational probe particles. The latter consist of colloidal particles containing two fluorescently labeled cores suited for tracking the particle's orientation. A comparison of the experimental data with event driven Brownian simulations gives insights into the system's structure and dynamics close to the glass transition and sheds new light onto the translation–rotation coupling. The data show that with increasing volume fractions, translational dynamics slows down drastically, whereas rotational dynamics changes very little. We find convincing agreement between simulation and experiments, even though the simulations neglect far-field hydrodynamic interactions. An additional analysis of the glass transition following mode coupling theory works well for the structural dynamics but indicates a decoupling of the diffusion of the smaller particle species. Shear stress correlations do not decorrelate in the simulated glass states and are not affected by rotational motion.

I. INTRODUCTION

At the colloidal glass transition, the flow properties of a dispersion change at the colloid scale.[1] A single colloid in a continuum fluid exhibits Brownian random motion, and the diffusion coefficients of translation and rotation D_t and D_r, respectively, are coupled according to the laws of Stokes, Einstein, Debye, and Perrin.[2,3] The solvent flow has to obey the condition of vanishing relative velocity on the surface of the colloid. Thus, random forces and torques are coupled, leading to a constant ratio $D_t/D_r^l = d^2/3$ for a sphere of diameter d, independent, for example, of the viscosity η of the dispersion. In the semi-dilute regime, the coupling of rotation and translation of colloids has been a topic of longstanding interest, especially the question whether the solvent or the dispersion viscosity sets the rotational diffusion coefficient.[4–9] At higher concentrations, the close relationship between rotation and translation gets lost when approaching solidification. The direction of the deviations depends on the type of liquid, the thermodynamic phases explored, and the kind of tracer particle studied.[10–16] In glass-forming liquids, the sensitivity of the rotation–translation coupling has been used to inspect local motion, which remains incompletely understood when approaching the glass transition. Large tracers in molecular fluids have shown a strong variation of the ratio of diffusivities in experiments and simulations: While rotational diffusion remains strongly coupled to viscosity, $D_r \propto 1/\eta$, translational diffusion decouples.[17,18] Investigations of colloidal dispersions promise to give further insights into these phenomena since individual particles can be tracked even at concentrations close to the glass transition.[19] A direct observation of their rotational motion close to the glass transition, however, has been possible only in two systems. Edmond *et al.* considered tetrahedral clusters of colloids in a hard sphere solution.[20] They observed that translational diffusion slows down less than rotational, which remains tied to structural relaxation. This is reminiscent of the molecular glass-forming liquids. A quite different behavior was observed with spherical Janus colloids,[21,22] where translational diffusion was found to slow down more strongly than rotational when the colloidal glass transition is approached. Clearly, the question of rotation–translation coupling at the colloidal glass transition remains intriguing.

Here, we report the results of experiments and simulations of the translation–rotation coupling of dispersions of spherical colloids near the colloidal glass transition and compare them to predictions from mode coupling theory (MCT).[23] Spherical colloids arguably are the simplest system as they can be described by the paradigmatic hard sphere fluid model. Crystallization can be prevented by mixing two species with appropriate size and concentration ratios. The dominant control parameter is the total volume fraction ϕ. Experiments were based on confocal fluorescence microscopy of dense dispersions of polymethyl methacrylate (PMMA) core/shell colloids with hard potentials. These dispersions were spiked with low concentrations of spherical PMMA colloids containing two cores as rotational probe particles.[14] From the fluorescence data, particle trajectories could be obtained simultaneously for translational and rotational diffusion. For the simulations, a rough sphere model was employed, which proved useful for understanding the collective angular motion in molecular fluids, and had been studied by theoretical and numerical methods.[24–29] It presumes that the spheres collide elastically and the relative velocity of the contact points reverts in the collision. Because there is no slip at the collision, the angular velocities of the collision partners get changed according to the conservation of total angular momentum. Varying the mass density distribution, the model has, for example, provided insights into the origin of different coefficients in the Stokes–Einstein relation in liquids,[30] and it is widely used in supercritical fluids.[31] This model of rough spheres can be tuned from the molecular scale, where atoms move ballistically, to the mesoscopic scale, where colloids perform Brownian motion. The model enables separation of the importance of interparticle correlations from the random forces and torques exerted by the solvent. Thus, the cooperativity of the translational and rotational motion can be tested. From experiments, it is known that particle roughness and long ranged solvent flow can become important.[32,33] Both are neglected in the simulation, and the comparison of the simulations with the experiment can elucidate whether the local coupling of rotation and translation dominates in dispersions of sterically stabilized hard colloids at packing fractions close to the glass transition. At higher packing fractions, additional phenomena may set in when approaching jamming.

Recently, long-ranged stress correlations in glass-forming colloidal dispersions have been predicted but not yet observed.[34,35] Employing the Brownian simulations after calibration to the experimental system, we explore the magnitude of the stress correlations in order to address the possibility of their measurement in glass-forming colloidal dispersions. We not only approach the colloidal glass transition but also enter the glass state where aging indicates that the system has fallen out of equilibrium. Quantitative Brownian dynamics simulations accompanying the experiments test the aging phenomena, verifying that a colloidal glass was prepared. The recorded mean square displacements indicate that large and small spheres are tightly localized, yet there still remains local free volume enabling fast translational and rotational motion. In the simulations, we can tune the Brownian noise and thereby see that angle variations get completely decorrelated by the random torques in a thermal heat bath, while molecular systems require many particle collisions before angular diffusion becomes effective. Finally, we also compare the results from experiment and simulation to mode coupling theory (MCT),[23] which predicts a glass transition value for our mixture, which is close to the observed one.[36] Within MCT, rotational motion of anisotropic particles was also considered, predicting a peculiar decoupling of even and odd angular momenta states for small aspect ratios,[37–39] which, however, lies at a finite aspect ratio and thus cannot be accessed with spherical particles.

This paper is organized as follows. In Sec. II, the system is introduced together with the experimental and simulational methods. In Sec. III, the results are presented, including radial distribution functions (RDFs), mean squared displacements (MSDs), and angular correlation functions for three different densities. Experimental data are analyzed and compared to data from the simulations. Section IV compares with MCT predictions and analyzes the emergence of elasticity. Conclusions and a discussion of the results are given in Sec. VI.

II. SETUPS

A. Experiment

The system studied in the experiments is based on a binary mixture of sterically stabilized PMMA/PMMA core/shell particles that were prepared following the procedure of Schütter *et al.*[14] (cf. Fig. 1). In brief, we first synthesized PMMA core particles with a diameter of 1 μm. The cores were copolymerized with either the BODIPY dye [4,4-difluoro-8-(4-methacrylatephenyl)-3,5-bis-(4-methoxyphenyl)-4-bora-3a,4a-diaza-s-indacene][40] or Quasar 670. Several seeded dispersion polymerization steps were employed to grow additional PMMA layers onto the cores to obtain particles with a final diameter of 2.08 μm [polydispersity index (PDI)

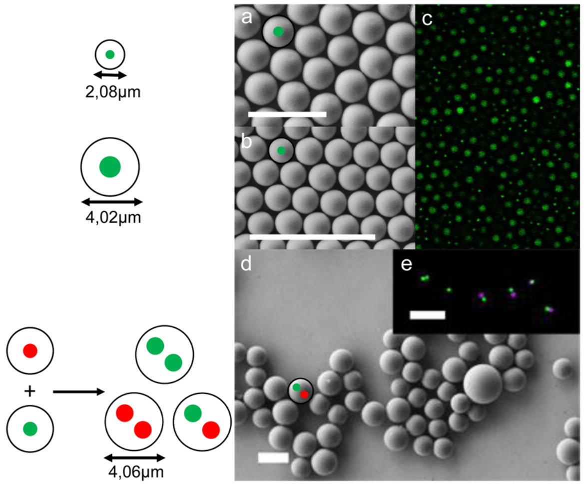

FIG. 1. Colloid dispersions consisted of PMMA/PMMA core/shell particles with differently labeled, fluorescent cores. To avoid crystallization, bidisperse mixtures of particles with diameters of 2.08 and 4.02 μm were used as a host system. Colloids with two cores and a diameter comparable to the larger host particles were added in high dilution and served as rotation probes. Scale bars are 10 μm in the SEM images (a) and (b), 5 μm in the SEM image (d), and 10 μm in the confocal fluorescence images (c) and (e).

of 5.1% determined from electron microscopy images] and 4.02 μm (PDI of 3.5%). Particles with two cores were synthesized by treating the particles with acetone.[14] Two-core particles with a diameter of 4.06 μm were employed as rotation probes. Several sedimentation steps were performed to reduce the number of particles with more than two cores as far as possible. For the preparation of the colloidal dispersions, the particles were dissolved in a density and refractive index matching mixture of cyclohexyl bromide saturated with tetrabutylammonium bromide and *cis*-decalin (85%:15%, w/w).[41] The number ratio of small particles, larger particles, and rotation probes was 100:100:1. The reported packing fraction measure the total volume taken by all colloidal particles. Steinhardt order parameters were determined to verify that colloidal glasses were prepared.[42]

Fluorescence images were acquired using a confocal fluorescence laser scanning microscope (TCS SP5, Leica Microsystems) with a resonant scanner (8000 Hz, bidirectional scanning mode) and a glycerol immersion objective (63× magnification, 1.3 NA). The microscope was temperature stabilized (Ludin Cube 2, Life Imaging Services) to 23 ± 0.5 °C. 3D-image stacks (1024 × 256 × 100 voxels) with pixel sizes of dx = dy = 141.3 nm and dz = 210 nm resulting in 3D image volumes of 144.7 × 36.2 × 21.0 μm^3 were recorded with a lag time of t = 5 s. The image stacks were recorded with distances of at least 25 μm to the sample chamber walls. To allow equilibration, all samples were put onto the objective 16 h before the measurements started. From the image stacks, trajectories for 3D-translation and rotation of the colloids were generated as described earlier.[43] To capture faster dynamics, we additionally performed 2D measurements in only one plane. Lag times for these measurements were t = 0.1 s.

B. Simulation

In order to interpret and analyze the experimental observations, we performed event driven Brownian dynamics (EBD) simulations of a binary hard sphere mixture.[44,45] Different from previous simulations of colloids, which neglected their rotational motion, we account for the coupling of rotation and translation via the flow of the solvent. In the EBD algorithm, the particles move with constant velocities $\boldsymbol{v}_i$ and angular velocities $\boldsymbol{\omega}_i$ between events according to Newton's first law. Diffusion is modeled by the Brownian thermostat, redistributing the particles' (angular) velocities at fixed "Brownian" time steps. Particle collisions encode the potential interactions.

Solvent-mediated interactions among the colloids, called hydrodynamic interactions, are instantaneous and affect the short-time diffusion of the particles.[2] The EBD algorithm neglects their long-ranged contribution as do other potential free algorithms of hard colloids.[46] For smooth spheres, this approximation has been tested and verified when approaching the colloidal glass transition.[47] Here, we account for the aspect of the local flow of solvent around the colloids to couple rotation and translation. We do this by two strategies, first by including the correct rotational and translational diffusion in the dilute limit, and, second, by collisions that account for forces and torques.

To model diffusion, we draw the component of the translational velocities in each spatial direction from a Gaussian distribution with zero mean and unit variance $v_0^2 = 1$ at fixed time steps τ_t (in Newtonian units this Maxwell–Boltzmann distribution corresponds to $v_0^2 = k_B T/m = 1$). Rotational diffusion is achieved by redrawing angular velocities every time step τ_r. Assuming a Maxwell–Boltzmann distribution of angular velocities for spheres with a moment of inertia $I_\zeta = \frac{1}{\alpha} m d_\zeta^2$, where $\zeta \in \{s, l\}$ denotes either small s or large l particles, d_ζ denotes the respective diameter, and α is a dimensionless number that encodes the mass distribution of the spheres, the angular variance becomes $\omega_{0,\zeta}^2 = \alpha/d_\zeta^2$ for the small and large particles. We assume a homogeneous mass distribution, which gives $\alpha = 10$. After many Brownian time steps, the mean squared translational displacements and angular displacements grow linearly with the number of steps and the (short-time) translational and rotational diffusion coefficients take the values $D_t = v_0^2 \tau_t/2$ and $D_r = \omega_0^2 \tau_r/2$. In order to recover the ratio of rotational and translational diffusion coefficients predicted by Stokes, Einstein, and Debye for dilute colloidal spheres,[2] $D_t/D_r^l = d_l^2/3$, the ratio between rotational and translational Brownian time steps thus needs to be chosen as[45]

$$\tau_t/\tau_r = \alpha/3. \tag{1}$$

At finite densities, the HS interact as perfectly rough elastic spheres.[24–29] This collision rule couples rotations and translations. It inverts the relative velocities of the contact points at collision $\boldsymbol{v}_c' = -\boldsymbol{v}_c$, as would hold for two colliding rubber balls. There is no slip of the two colliding surfaces. Before the collision, the contact points approach each other with velocity: $\boldsymbol{v}_c = \boldsymbol{v}_2 - \boldsymbol{v}_1 + \left(\frac{d_1}{2}\boldsymbol{\omega}_1 + \frac{d_2}{2}\boldsymbol{\omega}_2\right) \times \hat{\boldsymbol{n}}$ with the collision vector $\hat{\boldsymbol{n}} = (\boldsymbol{r}_1 - \boldsymbol{r}_2)/|\boldsymbol{r}_1 - \boldsymbol{r}_2|$. The relative velocity of the contact points after the collision, $\boldsymbol{v}_c'$, follows from the final velocities (marked by an apostrophe) given in the collision law:

$$\boldsymbol{v}_{1,2}' = \boldsymbol{v}_{1,2} \pm \Delta\boldsymbol{p}/m_{1,2}, \tag{2}$$

$$\boldsymbol{\omega}_{1,2}' = \boldsymbol{\omega}_{1,2} - \frac{d_{1,2}}{2I_{1,2}} \hat{\boldsymbol{n}} \times \Delta\boldsymbol{p}, \tag{3}$$

$$\Delta\boldsymbol{p} = \frac{2\mu}{1 + \mu\kappa} \left(\boldsymbol{v}_c + \mu\kappa(\boldsymbol{v}_c \cdot \hat{\boldsymbol{n}})\hat{\boldsymbol{n}}\right). \tag{4}$$

We introduced two convenient parameters, reduced mass $\mu = \frac{m_1 m_2}{m_1 + m_2}$ and reduced moment of inertia $\kappa = \frac{\alpha_1}{4m_1} + \frac{\alpha_2}{4m_2}$, which capture the collisions of spheres with different radii.

The shown time dependent data are averaged over roughly 100 systems, with particle numbers of $N = 1728$ up to $N = 8000$. The number ratio is $N_s/N_l = 1$, and the size ratio is $d_l = 2d_s$, as determined in the experiment. Only the density is varied. In order to sample the dynamics, the Brownian time step of translation is set to $\tau_t D_t/d_l^2 = 5 \times 10^{-7}$. It has to be chosen small enough so that the observation of short time diffusion in the MSD is possible before the caging regime appears. This is hard for the used packing fractions up to $\phi = 0.65$, explaining why we had to use such a small value for τ_t.

C. Equilibration and simulation preparation

As we study samples above the glass transition, the structural relaxation time is excessively long and aging affects the measurements. Thus, the protocol to prepare the simulated systems needs to be specified. The particles start as point particles from a simple cubic lattice and with initial velocities drawn from the described Gaussians. Then, they are propagated by Newtonian dynamics, i.e., there is no Brownian time step. Every fixed time step $\tau_i = 0.05 v_0/d_l$, all particles are inflated until they are in contact with their closest neighbor or they reached their maximum size.[48] Then, we proceeded with Newtonian dynamics and measured the decay of the coherent density correlation function at a wave vector magnitude of the position of the nearest neighbor peak in the static structure factor. This was possible for all shown densities, except for the highest two. The latter cases were stopped earlier because the waiting times increased drastically. We explicitly checked that for these two volume fractions, the data shown in Sec. III were stationary in the given time window. The waiting time $t_w = 0$ is measured as time span from the instance when all particles reach their prescribed radii, and with that, the prescribed density of the system is reached. The inflation process needs an increasing time span for increasing densities. For $\phi = 0.59$, this process finishes on average after $4.8 v_0/d_l$ and for $\phi = 0.65$ after $18.3 v_0/d_l$.

III. RESULTS

We present experimental data compared to simulation for three different densities: below, closely above, and clearly above the predicted MCT glass transition.[36] For the given size ratio and concentrations, microscopic MCT predicts $\phi_c^{\mathrm{MCT}} = 0.52$. Considering the tendency of MCT to overestimate the glass formation,[49,50] we estimate the experimental value to lie 15% higher, $\phi_c^{\mathrm{exp}} \approx 0.6$, and test it below. We compare the structure by presenting the RDF, the translational dynamics by measuring the MSD, and the rotational dynamics by showing averaged Legendre polynomials of the angular variation.

A. Crystallization

The phase diagram of the binary mixture studied in this work is investigated in Ref. 51. The authors report the appearance of AB_2 crystalline states for several densities. Within the density range explored in this work, crystalline states are reported for $\phi = 0.60$ and $\phi = 0.62$. For the experimental systems, Steinhardt order parameters[42] of fourth and sixth order were determined and showed no sign of crystalline order. To test for the possible formation of crystals in the simulated systems, we calculated bond order parameters of the final configurations. The coarse-grained bond order parameters are introduced in Ref. 52. To calculate the nearest neighbors, we follow the recipe outlined in Ref. 53. Our systems do not show signs of crystallization, neither the experimental samples nor the simulated systems. We attribute this to the difficult pathway to Laves-phase formation observed and overcome in Refs. 51 and 54.

B. Radial distribution functions

In order to characterize the dispersions and determine their structural parameters, we study the RDFs. Figure 2 shows the RDF results for increasing densities. The packing fraction of the upper panel corresponds to a fluid state, that of the central one to a state around the MCT glass transition, and the bottom panel shows data for a packing fraction deep in the glass state. For all densities, three next-neighbor peaks indicating the three distances of small–small, small–large, and large–large spheres are visible. Weak traces of these distances can also be seen at the second neighbor shells. While with increasing total packing fraction, the structuring in the RDF gets stronger, in no case, sharp peaks indicating crystalline order emerge. All states are thus fluid like. In general, the peaks in the simulation graphs are sharper than those in the experimental graphs. This points at the (small) polydispersity in the experimental sample. We use the RDF to calibrate the simulated systems to the experimental ones, for the following reasons: (i) The particles swell in the solvent. (ii) The assumption of a perfectly binary mixture does not hold for the experiment, where a small polydispersity exists. (iii) The determination of packing fractions of colloidal dispersions is error prone.[55] The first problem is overcome by choosing a single length scale, the diameter of the large species d_l, when comparing simulation and experiment. The experimental RDF data originally measured in μm are scaled by the value $d_l = 4.76\ \mu$m, which visually provides the best fit. This value indicates an appreciable swelling of the particles in solution. The simulated packing fractions, chosen for the fits, then turn out very close to the experimentally determined values. The remaining differences between simulation and experiment are considered to arise from particle polydispersity and from the problem to measure ϕ precisely.

Overall, a very good mapping between the structures as captured in the two-component radial distribution functions is observed between simulation and experiment. As seen in many investigations of glass-forming systems, the structure changes only smoothly when crossing the colloidal glass transition.[1]

C. Mean squared displacements

After having studied the structure, we now turn to the dynamics of the system. Figure 3 depicts the MSDs $\delta r_\alpha^2 = \langle (\boldsymbol{r}_\alpha(t) - \boldsymbol{r}_\alpha(0))^2 \rangle$, where α denotes the particle species and colored symbols indicate the experimental data. The systems are the same as those shown in Fig. 2. The upper curves in each plot are MSDs from small host particles, whereas the lower ones originate from the large host particles. The experimental short time data were determined from 2D measurements, while data for longer times were extracted from 3D measurements. The two measurements are denoted by different colors. The simulation curves are drawn in black.

While Sec. III B showed that the structure of the binary mixture changed smoothly with increasing packing fraction, the plateaus in the MSD data highlight that the colloid motion slows down strongly.[1,56] This is caused by the trapping of the colloids in the cages of their neighbors for intermediate times. The finite lifetime plateau indicates incipient localization, and a localization length following Lindemann's discussion[57] of crystal melting could be read-off. This is emphasized by the purple bar in Fig. 3(b), denoting the explicit value of $\delta r^2(t \to \infty)$ according to Lindemann's criterion evaluated in MCT.[58] Yet, determining the long-time diffusivity is difficult because of the finite time-window of experimental observation and because of possible aging effects. Here, the simulations can help us interpret the dynamics, because the waiting time can be controlled, and additional states can be sampled.

Since the particle diameter was taken from the RDF comparison, the MSDs can be plotted in re-scaled form $\delta r_\alpha^2/d_l^2$ with $d_l^2 = (4.76\ \mu\mathrm{m})^2$. As the packing fractions have also been determined in the fits of the RDFs, the only parameter to match the

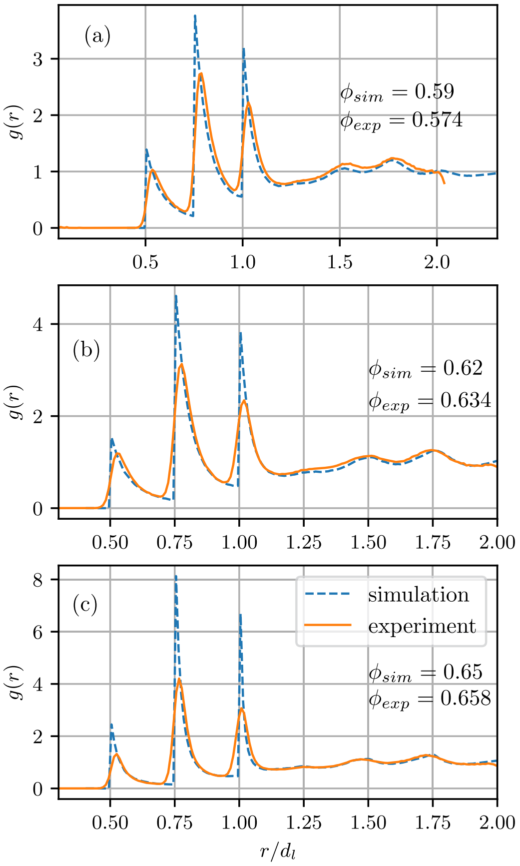

FIG. 2. Radial distribution functions $g(r)$ of the colloidal mixtures (orange solid lines) compared to the ones from simulation (blue dashed lines). The volume fractions ϕ correspond to systems below, close to, and above the MCT glass transition.

time-dependent data from simulation and experiment is the time scale d_l^2/D_t, given by the translational short-time diffusion coefficient. Best agreement was achieved by rescaling experimental data by

$$D_t^{\text{exp}}/d_l^2 = 0.001 \text{ s}^{-1}. \tag{5}$$

Figure 3(a) shows the diffusion in a colloidal fluid state. Long-time diffusion of both particle species is clearly attained at long times. At intermediate times, a plateau in the MSDs starts developing, which indicates the incipient localization of the colloids. As expected, the larger colloids move less than the smaller ones, and the gap widens with increasing time. At the intermediate packing fraction $\phi_{\text{exp}} = 0.634$, the MSDs have slowed down, and long-time diffusion of the large colloids cannot be seen in the experimental window anymore. Yet, the apparent diffusion of the smaller colloids at long times suggests that the state could be fluid. This is, however, not supported by the simulations at this packing fraction. The system at $\phi_{sim} = 0.62$ cannot be equilibrated and exhibits a structural relaxation time that grows with waiting time t_w. The simulation curve shown in Fig. 3(b) was measured after Newtonian propagation for $t_w = 19\,000 d_l/v_0$. The MSDs in the time window shown in Fig. 3(b), however, are already stationary and do not change with increasing t_w. Data for a density far above the predicted MCT-glass transition are depicted in Fig. 3(c). In this case, aging effects would not come as a surprise. They are, indeed, observed in the simulations, shown by the magenta line. We simulated a system that was equilibrated by using the standard inflation protocol and then followed by Newtonian dynamics for $t_w = 1000 d_l/v_0$. This reproduces the earlier onset of the α-relaxation in the experiment very well. For longer waiting times, however, the escape out of the cage takes longer. In Fig. 3(c), the black curve shows the MSD of a system that aged for $t_w = 16\,000 d_l/v_0$, whereas for larger t_w, no aging effects remain in the studied time window.

Concluding the comparison of the translational dynamics, one can summarize that very good agreement between experiment and

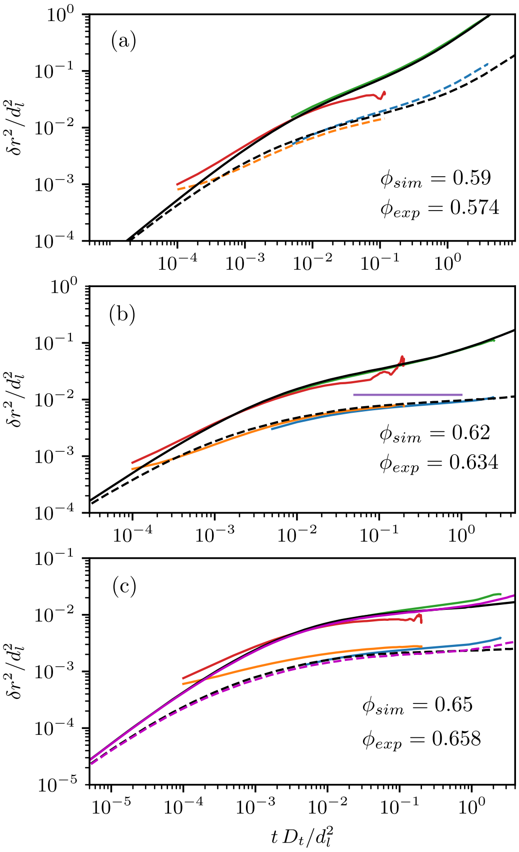

FIG. 3. MSD of small (upper curves) and big particles (lower curves) in experiment (colored symbols) and simulation (black lines) for the densities where RDFs are shown in Fig. 2. Experimental data at short times are from 2D confocal scans, while 3D scans gave the data at long times. In panel (b), a bar gives Lindemann's criterion, and in panel (c), the magenta line shows simulation data of a system that was given less time for equilibration (see the text). At short times, the experimental data converge to the positioning accuracy, explaining the deviations from the simulated data.[43]

simulation can be achieved by a mere tuning of the short-time diffusion coefficient and transferring all other parameters from the structural comparison.

D. Rotational dynamics

To quantify the rotational dynamics, we calculate Legendre polynomials L_n of the angle variation of the tracer. The second polynomial, which can also be measured by depolarized light scattering,[59] reads

$$L_2(t) = \left\langle \frac{3}{2}\left(\cos\left(\theta(t)\right)\right)^2 - \frac{1}{2} \right\rangle, \tag{6}$$

where we chose $\theta(0) = 0$ for each particle. The idealized case of diffusion on a sphere yields[60]

$$L_n(t) = \exp\left(-n\,(n+1)\,D_r\,t\right). \tag{7}$$

Experiment and free diffusion are compared in Fig. 4. The ratio of the rotational and translational diffusion coefficients of a single spherical colloid of diameter d_l is given by the Stokes–Einstein–Debye and Stokes–Einstein relations to $D_t/D_r^l = d_l^2/3$. From Eq. (5), we can then predict the free rotation coefficient of the experiment to read

$$D_r^l = 0.003\ \mathrm{s}^{-1}. \tag{8}$$

The black dashed theory slope in Figs. 4(a) and 4(b) is calculated with Eqs. (7) and (8). From this, it can be concluded that rotational diffusion close to the glass transition is still very similar to rotational diffusion of a dilute sphere. Figure 4(b) shows the fourth Legendre polynomial, which is affected by smaller angle variations and thus records somewhat larger differences to Debye's free rotational diffusion.

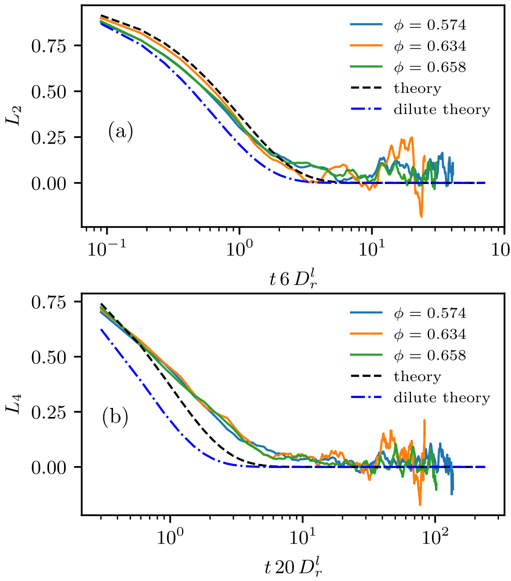

FIG. 4. Experimental angular correlation function L_2 [in panel (a)] and L_4 [in panel (b)] for different densities. The black dashed line "theory" gives the free Brownian rotation equation (7), where D_r is calculated from the short-time translational diffusion (8) at this ϕ. The blue dotted-dashed line uses the dilute rotational diffusion coefficient. The density dependence is very weak, especially compared to the extreme sensitivity of the MSDs in this density range. Note the different scaling of the time axis.

Considering the strong slowing down of the translational motion shown in Fig. 3, the findings in Fig. 4 state, by contrast, that the rotational diffusion of a sphere is not affected by the packing fraction. This holds true even in the extreme case when crossing the colloidal glass transition. In the limit $\phi \to 0$, the rotational diffusion is that of a free rotor and it remains that of a free rotor at any measured density. There is a slight subtlety, though, arising from the solvent mediated hydrodynamic interactions, which make D_t and D_r slightly density dependent. The blue dashed lines in Fig. 4 are calculated using Eq. (7) with D_r^l directly taken from measurements of dilute tracer particles. It does not agree as well with the measured data because the increased particle density has changed the local friction experienced by the colloids. This is captured in the small density-dependence of the short-time rotational diffusion constant, while the long-time diffusion constant does not change relative to this short-time one.

Simulation results at $\phi = 0.65$ are shown in Fig. 5. We see perfect agreement between the theory of free Brownian rotation and simulation. This can be rationalized because we choose τ_t smaller than the mean collision time to produce proper short time diffusion. From Eq. (1), it follows that τ_r is even smaller. So, the rotational Brownian events of the thermostat are much more frequent than collisions with other particles. The mean collision time at $\phi = 0.65$ in BD is $\tau_c = 40 \cdot 10^{-7}\,D_t/d_l^2$, which means a rotational thermostat event is roughly 26 times more frequent than a collision. This implies that the thermostat wipes out the effect of the collisions on the rotational diffusion. To this point, one could argue that this is the same for the translations as well, because translational velocities are also resampled eight times more often than collisions happen on average. Yet, this clarifies the essence of the cooperative cage effect: The translation of a spherical tracer is hindered by the surrounding particles, and diffusion requires a collective rearrangement. This leads to long-lasting memory in the particle collisions that are not destroyed by random velocity changes. By contrast, the rotation of a sphere does not require extra volume (in contrast to, for instance, tetrahedra[20] or ellipsoids,[61] or particles at interfaces[62]). Thus, the rotation of a sphere does not couple to the cage of the surrounding particles and no (strong) excluded volume effects are observed for rotational diffusion.

IV. MCT GLASS TRANSITION ANALYSIS

In order to estimate the glass transition point, we performed an α-scaling analysis following the predictions from MCT. It predicts a scaling of the density autocorrelation (ACF) function, $S(q,t) = \left\langle \rho(\boldsymbol{q},t)^* \rho(\boldsymbol{q},0) \right\rangle$, during the decay from the plateau (α-relaxation) for packing fractions approaching the MCT glass transition ϕ_c^{MCT}.[23] Here, $\rho(\boldsymbol{q},t) = N^{-1/2}\sum_{j=1}^{N} \exp\left(i\boldsymbol{q}\cdot\boldsymbol{r}_j(t)\right)$ is the fluctuating microscopic density.

Figure 6 shows the re-scaled density ACF for different densities; for efficiency, the Brownian time step is in this section increased to $\tau_t\,D_t/d_l^2 = 5 \times 10^{-5}$. The predicted α-scaling is well confirmed by the

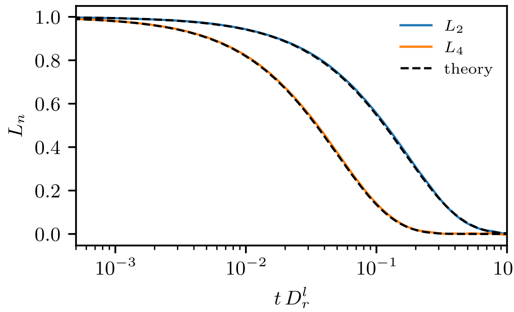

FIG. 5. Simulation results for the rotational correlation functions [Eq. (6)] of the large particles. The dashed lines show the theory of the free rotation (7).

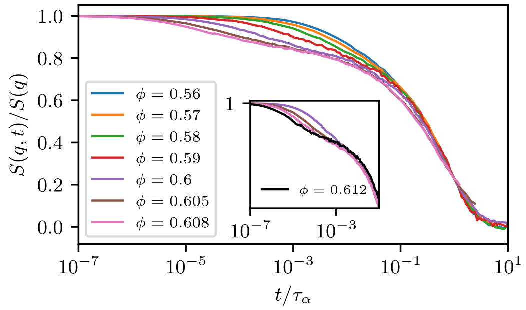

FIG. 6. Normalized collective density ACF at $q\,d_l = 7.9$. Re-scaled so that a unit time marks a decay to 0.23. The graphs collapse almost perfectly. The α-relaxation times extracted from this figure are shown in Fig. 7. The inset includes a correlator at $\phi = 0.612 > \phi_c^{\text{sim}}$, which violates scaling and cuts the emerging scaling function.

simulations. MCT predicts an algebraic divergence of the relaxation times $\tau_\alpha(\phi)$ toward the glass transition,

$$\tau_\alpha = C \cdot |\phi - \phi_c|^{-\gamma} \tag{9}$$

with an MCT-exponent $\gamma = 2.6477$ depending on the parameters of the binary mixture, such as number and size ratios. The quoted value corresponds to size ratio $d_l/d_s = 2$ and equal concentrations $N_l/N_s = 1$.[36] As can be seen in Fig. 7, the divergence is well confirmed by the relaxation times taken from the total, see Fig. 6, and the species-resolved density ACF. In each case, the wave vector corresponds to the average particle separation. The power-law behavior leads to the estimate $\phi_c^{\text{sim}} = 0.612$. In the inset of Fig. 6, a correlator at packing fraction $\phi = 0.612 \geq \phi_c^{\text{sim}}$ is included, where the plateau value already increases above the one at $\phi = 0.605$, i.e., scaling is no longer possible as discussed in Refs. 63 and 64. The corresponding relaxation times at $\phi = 0.612$ shown in Fig. 7 deviate from the algebraic divergence and hint toward an avoided ideal MCT glass transition.[65]

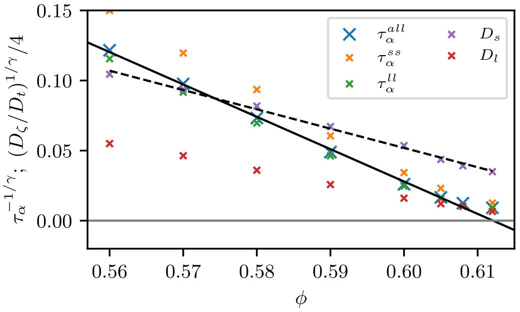

FIG. 7. Relaxation times of the total and partial density correlation functions from Fig. 6. By plotting $\tau_\alpha^{-1/\gamma}$, the algebraic law from Eq. (9) is given by a linear graph. The linear fit to the relaxation times predicts a glass transition of $\phi_c^{\text{sim}} = 0.612$. The relaxation time at $\phi = 0.612$ is excluded from this fit. A similar fit on $D_s^{1/\gamma}$ predicts a significantly higher divergence at $\phi = 0.638$.

The MCT analysis in Fig. 6 includes the diffusion coefficients obtained from the MSD of small and large spheres. The diffusion of the large spheres is strongly coupled to the structural relaxation, but the smaller particles appear not to arrest with the structure at the same packing fraction. D_s rather appears to vanish at an appreciably higher packing fraction. In Ref. 66, the relation between the appearance of dynamical heterogeneities and the decoupling of coherent and incoherent time scales is discussed. The data in Fig. 7 show the decoupling in the form of different power-law divergences for D_ζ and τ_α. This is especially apparent for the small particles, where the collective relaxation time τ_α^{ss} approaches the same singularity as the one of the big spheres τ_α^{bb}, while D_s vanishes at an appreciably higher packing fraction of $\phi = 0.638$. This follows when the black dashed fitted slope in Fig. 7 is extrapolated to zero.

V. SHEAR MODULUS

Recently, the rheology of rough colloids has been discussed in the context of shear thickening caused by frictional contacts.[67–71] Thus, it is of interest to compare the shear moduli of rough and smooth spheres, which can be done using the standard Brownian dynamics algorithm[44,45] and our modified one. The shear modulus is given by the ACF of the shear stresses $\sigma_{\alpha\beta}(t)$,

$$G(t) = \frac{V}{k_B\,T}\frac{1}{3}\sum_{\alpha<\beta}\left\langle \sigma_{\alpha\beta}(t)\sigma_{\alpha\beta}(0)\right\rangle. \tag{10}$$

In the smooth sphere case, the shear stresses come from collisions, which are instantaneous and binary.[72,73] For the considered system with rotational degrees of freedom, the stress tensor is in general not symmetric but can be symmetrized following Ref. 74. Then, the stress tensor reads

$$\sigma_{\alpha\beta}(t) = \frac{1}{\Delta\tau_c V}\sum_{\tau_c}\frac{1}{2}\{\Delta \boldsymbol{p}_\alpha \Delta \boldsymbol{r}_\beta + \Delta \boldsymbol{p}_\beta \Delta \boldsymbol{r}_\alpha\}. \tag{11}$$

Here, $\Delta\tau_c$ denotes the time window, over which we average the collisions. The sum runs over all collisions, happening in the time interval $t \in [t - \Delta\tau_c/2, t + \Delta\tau_c/2]$. $\Delta\boldsymbol{r}$ denotes the center to center vector of the two colliding particles, and $\Delta\boldsymbol{p}$ denotes the transferred momentum.

The time-dependent shear modulus $G(t)$ does not show any differences between smooth and rough spheres. For the density above the glass transition, the modulus does not decay in the simulated time window and rather approaches a long time plateau (marked by a horizontal bar in Fig. 8), while it decays to zero in

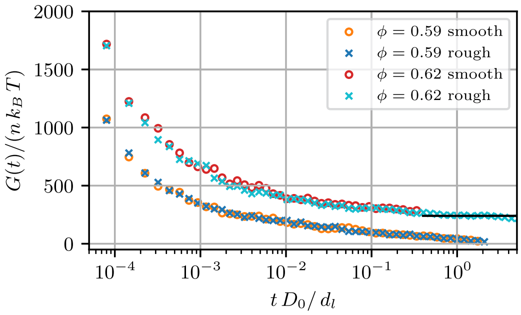

FIG. 8. Time-dependent shear modulus $G(t)$ is shown for the binary mixtures of the rough and the corresponding smooth spheres at a fluid and a glass volume fraction; see the legend. The shear elastic constant of the glass states is marked by a horizontal bar at $G_\infty/(nk_BT) = 240$.

the liquid. The lack of a difference suggests that appreciable asperities are required in order for frictional forces to lock the rotational motion. The amplitude G_∞ of the shear stress correlations frozen-in in the glass state gives the shear modulus,[75,76] which sets the scale of the long-ranged stress fluctuations in glass-forming dispersions.[34,35] It is clearly of entropic origin and scales with the thermal energy per particle, $G_\infty = \alpha k_B T(N/V)$. Figure 8 shows that the prefactor is large compared to unity, $\alpha \approx 240$.

VI. DISCUSSION

We have reported simultaneous measurements of the rotation and translational dynamics of a binary colloidal dispersion in the vicinity of its glass transition. The rotations of tailor-made fluorescently labeled multi-core shell tracers could be tracked at very high densities. While the diffusion of large and small particles essentially freezes at the glass transition, the rotations show only a weak dependence on density. This can be rationalized, as the particles are spherical and, therefore, do not need additional free volume to rotate, while displacements get suppressed by the collective cage effect.

We performed Brownian event driven simulations modeling the binary mixture precisely, i.e., taking the size and concentration ratios from experiment. The simulation approach tailored to hard sphere interactions is potential free and mimics local hydrodynamic forces and torques between different particles. The solvent enters the simulation as a Brownian thermostat, which leads to the correct rotational and translational diffusion of an isolated colloid, viz., the Stokes–Einstein–Debye diffusion coefficients. At finite densities, rotation–translation coupling is included in binary collisions, where momentum- and angular momentum-transfer model short-ranged forces and torques. We consider this to mimic lubrication forces transmitted by the solvent. Despite these simplifications, experiment and simulations agree well, considering slow translational diffusion and fast rotational decorrelation.

For the MSD of the highest density, the earlier onset of long time diffusion could be rationalized by aging effects. The simulations show that Brownian fluctuations induced by the solvent, at least as modeled in our scattering law, dominate the initial decorrelation of displacements and angles. However, long-term memory is only encoded in the particle structure not in the solvent flow. The angular motion thus does not couple to the slow cooperative structural rearrangement.

Recently, the emergence of long-ranged stress correlations at the glass transition has been predicted.[34] This requires the macroscopic shear modulus to become slow because it sets the amplitudes of the stress correlations. The simulations indicate that the shear modulus per particle by far exceeds thermal energy close to the glass transition and that rotational motion has no consequences on the rheology of the investigated dispersions.

In addition to experiments and simulations, we performed an α-scaling analysis of the simulated density correlation function that provided an estimate of the MCT glass transition of $\phi_c^{sim} = 0.61$, which should be compared to the predicted value $\phi_c^{MCT} = 0.52$. The difference for the considered mixture is similar to the one obtained for slightly polydisperse colloidal hard spheres.[49] The algebraic divergence of relaxation times predicted by MCT agrees well with simulations of the local density fluctuations. Yet, the very different mobilities of the two species cannot be neglected. The smaller colloids decouple from the glassy structural relaxation and remain rather mobile around ϕ_c^{sim}. We also observe stronger aging of the large particles compared to the small ones. This decoupling was already observed in a unimodal system with a broad size distribution.[77] In contrast to Ref. 77, however, the glass transition of the large spheres is not smeared out but remains sharp in our case. For even larger size disparity, experiments[78] and simulation[79] found a qualitative difference in large and small particle motion and anomalous sub-diffusion of the latter. Even though we report a decoupling of small and large particles' diffusion, we see the same caging and structural arrest for both species.

ACKNOWLEDGMENTS

We thank Thomas Voigtmann for discussions and MCT calculations of binary mixtures. This work was supported by the Deutsche Forschungsgemeinschaft (DFG) via Grant No. SFB 1432 Project No. C07.

AUTHOR DECLARATIONS

Conflict of Interest

The authors have no conflicts to disclose.

Author Contributions

John Geiger: Data curation (equal); Formal analysis (equal); Investigation (equal); Software (equal). **Niklas Grimm**: Conceptualization (equal); Data curation (equal); Formal analysis (equal); Investigation (equal); Methodology (equal); Software (equal); Writing – original draft (equal); Writing – review & editing (equal). **Matthias Fuchs**: Conceptualization (equal); Formal analysis (equal); Funding acquisition (equal); Investigation (equal); Project administration (equal); Supervision (equal); Writing – original draft (equal); Writing – review & editing (equal). **Andreas Zumbusch**: Conceptualization (equal); Formal analysis (equal); Funding acquisition (equal); Project administration (equal); Supervision (equal); Writing – original draft (equal); Writing – review & editing (equal).

DATA AVAILABILITY

The data that support the findings of this study are available from the corresponding author upon reasonable request.

REFERENCES

[1] G. L. Hunter and E. R. Weeks, "The physics of the colloidal glass transition," Rep. Prog. Phys. **75**, 066501 (2012).

[2] J. K. G. Dhont, *An Introduction to Dynamics of Colloids* (Elsevier, Amsterdam, 1996).

[3] G. Koenderink, H. Zhang, D. Aarts, M. Lettinga, A. Philipse, and G. Nägele, "On the validity of Stokes-Einstein-Debye relations for rotational diffusion in colloidal suspensions," Faraday Discuss. **123**, 335 (2003).

[4] R. Jones, "Rotational diffusion of a tracer colloid particle: II. Long time orientational correlations," Physica A **157**, 752 (1989).

[5] B. U. Felderhof and R. B. Jones, "Orientational relaxation in a colloidal suspension of spheres," Phys. Rev. E **48**, 1084 (1993).

[6] V. Degiorgio, R. Piazza, and T. Bellini, "Static and dynamic light scattering study of fluorinated polymer colloids with a crystalline internal structure," Adv. Colloid Interface Sci. **48**, 61 (1994).

[7] M. P. Lettinga, C. M. van Kats, and A. P. Philipse, "Rotational diffusion of tracer spheres in packings and dispersions of colloidal spheres studied with time-resolved phosphorescence anisotropy," Langmuir **16**, 6166 (2000).

[8] S. Poblete, A. Wysocki, G. Gompper, and R. G. Winkler, "Hydrodynamics of discrete-particle models of spherical colloids: A multiparticle collision dynamics simulation study," Phys. Rev. E **90**, 033314 (2014).

[9] M. P. Lettinga, G. H. Koenderink, B. W. M. Kuipers, E. Bessels, and A. P. Philipse, "Rotational dynamics of colloidal spheres probed with fluorescence recovery after photobleaching," J. Chem. Phys. **120**, 4517 (2004).

[10] M. Roos, M. Ott, M. Hofmann, S. Link, E. Rössler, J. Balbach, A. Krushelnitsky, and K. Saalwächter, "Coupling and decoupling of rotational and translational diffusion of proteins under crowding conditions," J. Am. Chem. Soc. **138**, 10365 (2016).

[11] L. C. Hsiao, I. Saha-Dalal, R. G. Larson, and M. J. Solomon, "Translational and rotational dynamics in dense suspensions of smooth and rough colloids," Soft Matter **13**, 9229 (2017).

[12] B. Ilhan, F. Mugele, and M. H. G. Duits, "Roughness induced rotational slowdown near the colloidal glass transition," J. Colloid Interface Sci. **607**, 1709 (2022).

[13] D. J. Chun, Y. Oh, and B. J. Sung, "Translation-rotation decoupling of tracers reflects medium-range crystalline order in two-dimensional colloid glasses," Phys. Rev. E **104**, 054615 (2021).

[14] S. Schütter, J. Roller, A. Kick, J.-M. Meijer, and A. Zumbusch, "Real-space imaging of translational and rotational dynamics of hard spheres from the fluid to the crystal," Soft Matter **13**, 8240 (2017).

[15] S.-H. Chong and W. Kob, "Coupling and decoupling between translational and rotational dynamics in a supercooled molecular liquid," Phys. Rev. Lett. **102**, 025702 (2009).

[16] S. Vivek and E. R. Weeks, "Decoupling of translational and rotational diffusion in quasi-2D colloidal fluids," J. Chem. Phys. **147**, 134502 (2017).

[17] F. Fujara, B. Geil, H. Sillescu, and G. Fleischer, "Translational and rotational diffusion in supercooled orthoterphenyl close to the glass transition," Z. Phys. B: Condens. Matter **88**, 195 (1992).

[18] M. T. Cicerone, F. R. Blackburn, and M. D. Ediger, "How do molecules move near T_g? Molecular rotation of six probes in *o*-terphenyl across 14 decades in time," J. Chem. Phys. **102**, 471 (1995).

[19] E. R. Weeks, J. C. Crocker, A. C. Levitt, A. Schofield, and D. A. Weitz, "Three-dimensional direct imaging of structural relaxation near the colloidal glass transition," Science **287**, 627 (2000).

[20] K. Edmond, M. Elsesser, G. Hunter, D. Pine, and E. Weeks, "Decoupling of rotational and translational diffusion in supercooled colloidal fluids," Proc. Natl. Acad. Sci. U. S. A. **109**, 17891 (2012).

[21] S. M. Anthony, L. Hong, M. Kim, and S. Granick, "Single-particle colloid tracking in four dimensions," Langmuir **22**, 9812 (2006).

[22] M. Kim, S. M. Anthony, S. C. Bae, and S. Granick, "Colloidal rotation near the colloidal glass transition," J. Chem. Phys. **135**, 054905 (2011).

[23] W. Götze, *Complex Dynamics of Glass-Forming Liquids A Mode-Coupling Theory* (Oxford University Press, Oxford, 2009).

[24] D. Chandler, "Translational and rotational diffusion in liquids. I. Translational single-particle correlation functions," J. Chem. Phys. **60**, 3500 (1974).

[25] D. Chandler, "Translational and rotational diffusion in liquids. II. Orientational single-particle correlation functions," J. Chem. Phys. **60**, 3508 (1974).

[26] D. Chandler, "Rough hard sphere theory of the self-diffusion constant for molecular liquids," J. Chem. Phys. **62**, 1358 (1975).

[27] J. Lyklema, "Computer simulations of a rough sphere fluid I," Physica A **96**, 573 (1979).

[28] B. J. Berne, "Molecular dynamics of the rough sphere fluid. II. Kinetic models of partially sticky spheres, structured spheres, and rough screwballs," J. Chem. Phys. **66**, 2821 (1977).

[29] C. S. Pangali and B. J. Berne, "Molecular dynamics of the rough sphere fluid. III. The dependence of translational and rotational motion on particle roughness," J. Chem. Phys. **67**, 4571 (1977).

[30] O. Kravchenko and M. Thachuk, "The effect of rotational and translational energy exchange on tracer diffusion in rough hard sphere fluids," J. Chem. Phys. **134**, 114310 (2011).

[31] I. Medina, "Determination of diffusion coefficients for supercritical fluids," J. Chromatogr. A **1250**, 124 (2012).

[32] T. Yanagishima, Y. Liu, H. Tanaka, and R. P. A. Dullens, "Particle-level visualization of hydrodynamic and frictional couplings in dense suspensions of spherical colloids," Phys. Rev. X **11**, 021056 (2021).

[33] G. Koenderink, M. Lettinga, and A. Philipse, "Rotational dynamics of charged colloidal spheres: Role of particle interactions," J. Chem. Phys. **117**, 7751 (2002).

[34] M. Maier, A. Zippelius, and M. Fuchs, "Emergence of long-ranged stress correlations at the liquid to glass transition," Phys. Rev. Lett. **119**, 265701 (2017).

[35] F. Vogel, A. Zippelius, and M. Fuchs, "Emergence of Goldstone excitations in stress correlations of glass-forming colloidal dispersions," Europhys. Lett. **125**, 68003 (2019).

[36] T. Voigtmann, "Multiple glasses in asymmetric binary hard spheres," Europhys. Lett. **96**, 36006 (2011).

[37] R. Schilling and T. Scheidsteger, "Mode coupling approach to the ideal glass transition of molecular liquids: Linear molecules," Phys. Rev. E **56**, 2932 (1997).

[38] T. Franosch, M. Fuchs, W. Götze, M. R. Mayr, and A. P. Singh, "Theory for the reorientational dynamics in glass-forming liquids," Phys. Rev. E **56**, 5659 (1997).

[39] S.-H. Chong, A. J. Moreno, F. Sciortino, and W. Kob, "Evidence for the weak steric hindrance scenario in the supercooled-state reorientational dynamics," Phys. Rev. Lett. **94**, 215701 (2005).

[40] M. Baruah, W. Qin, N. Basarić, W. M. De Borggraeve, and N. Boens, "BODIPY-based hydroxyaryl derivatives as fluorescent pH probes," J. Org. Chem. **70**, 4152 (2005).

[41] A. Yethiraj and A. van Blaaderen, "A colloidal model system with an interaction tunable from hard sphere to soft and dipolar," Nature **421**, 513 (2003).

[42] P. J. Steinhardt, D. R. Nelson, and M. Ronchetti, "Bond-orientational order in liquids and glasses," Phys. Rev. B **28**, 784 (1983).

[43] J. Roller, P. Pfleiderer, J.-M. Meijer, and A. Zumbusch, "Detection and tracking of anisotropic core-shell colloids," J. Phys.: Condens. Matter **30**, 395903 (2018).

[44] A. Scala, T. Voigtmann, and C. De Michele, "Event-driven Brownian dynamics for hard spheres," J. Chem. Phys. **126**, 134109 (2007).

[45] F. Romano, C. De Michele, D. Marenduzzo, and E. Sanz, "Monte Carlo and event-driven dynamics of Brownian particles with orientational degrees of freedom," J. Chem. Phys. **135**, 124106 (2011).

[46] D. Heyes and J. Melrose, "Brownian dynamics simulations of model hard-sphere suspensions," J. Non-Newtonian Fluid Mech. **46**, 1 (1993).

[47] S. Marenne, J. F. Morris, D. R. Foss, and J. F. Brady, "Unsteady shear flows of colloidal hard-sphere suspensions by dynamic simulation," J. Rheol. **61**, 477 (2017).

[48] B. D. Lubachevsky and F. H. Stillinger, "Geometric properties of random disk packings," J. Stat. Phys. **60**, 561–583 (1990).

[49] W. van Megen, S. M. Underwood, and P. N. Pusey, "Nonergodicity parameters of colloidal glasses," Phys. Rev. Lett. **67**, 1586 (1991).

[50] M. Nauroth and W. Kob, "Quantitative test of the mode-coupling theory of the ideal glass transition for a binary Lennard-Jones system," Phys. Rev. E **55**, 657 (1997).

[51] P. K. Bommineni, M. Klement, and M. Engel, "Spontaneous crystallization in systems of binary hard sphere colloids," Phys. Rev. Lett. **124**, 218003 (2020).

[52] W. Lechner and C. Dellago, "Accurate determination of crystal structures based on averaged local bond order parameters," J. Chem. Phys. **129**, 114707 (2008).

[53] J. A. van Meel, L. Filion, C. Valeriani, and D. Frenkel, "A parameter-free, solid-angle based, nearest-neighbor algorithm," J. Chem. Phys. **136**, 234107 (2012).

[54] N. Schaertl, D. Botin, T. Palberg, and E. Bartsch, "Formation of Laves phases in buoyancy matched hard sphere suspensions," Soft Matter **14**, 5130 (2018).

[55] W. C. K. Poon, E. R. Weeks, and C. P. Royall, "On measuring colloidal volume fractions," Soft Matter **8**, 21 (2012).

[56] S. R. Williams and W. van Megen, "Motions in binary mixtures of hard colloidal spheres: Melting of the glass," Phys. Rev. E **64**, 041502 (2001).

[57] J. L. Barrat, W. Götze, and A. Latz, "The liquid-glass transition of the hard-sphere system," J. Phys.: Condens. Matter **1**, 7163 (1989).

[58] U. Bengtzelius, W. Götze, and A. Sjölander, "Dynamics of supercooled liquids and the glass transition," J. Phys. C: Solid State Phys. **17**, 5915 (1984).

[59] M. Hoffmann, C. S. Wagner, L. Harnau, and A. Wittemann, "3D Brownian diffusion of submicron-sized particle clusters," ACS Nano **3**, 3326 (2009).

[60] B. Berne and R. Pecora, *Dynamic Light Scattering* (Dover Publications, New York, 2000).

[61] J. Roller, A. Laganapan, J.-M. Meijer, M. Fuchs, and A. Zumbusch, "Observation of liquid glass in suspensions of ellipsoidal colloids," Proc. Natl. Acad. Sci. U. S. A. **118**, e2018072118 (2021).

[62] V. Niggel, M. R. Bailey, C. van Baalen, N. Zosso, and L. Isa, "3-D rotation tracking from 2-D images of spherical colloids with textured surfaces," Soft Matter **19**, 3069 (2023).

[63] F. Weysser and D. Hajnal, "Tests of mode-coupling theory in two dimensions," Phys. Rev. E **83**, 041503 (2011).

[64] S. Frey, F. Weysser, H. Meyer, J. Farago, M. Fuchs, and J. Baschnagel, "Simulated glass-forming polymer melts: Dynamic scattering functions, chain length effects, and mode-coupling theory analysis," Eur. Phys. J. E **38**, 11 (2015).

[65] W. Götze and L. Sjögren, "The glass transition singularity," Z. Phys. B: Condens. Matter **65**, 415 (1987).

[66] F. Weysser, A. M. Puertas, M. Fuchs, and T. Voigtmann, "Structural relaxation of polydisperse hard spheres: Comparison of the mode-coupling theory to a Langevin dynamics simulation," Phys. Rev. E **82**, 011504 (2010).

[67] N. Y. C. Lin, B. M. Guy, M. Hermes, C. Ness, J. Sun, W. C. K. Poon, and I. Cohen, "Hydrodynamic and contact contributions to continuous shear thickening in colloidal suspensions," Phys. Rev. Lett. **115**, 228304 (2015).

[68] C.-P. Hsu, S. N. Ramakrishna, M. Zanini, N. D. Spencer, and L. Isa, "Roughness-dependent tribology effects on discontinuous shear thickening," Proc. Natl. Acad. Sci. U. S. A. **115**, 5117 (2018).

[69] B. Schroyen, C.-P. Hsu, L. Isa, P. Van Puyvelde, and J. Vermant, "Stress contributions in colloidal suspensions: The smooth, the rough, and the hairy," Phys. Rev. Lett. **122**, 218001 (2019).

[70] S. Jamali and J. F. Brady, "Alternative frictional model for discontinuous shear thickening of dense suspensions: Hydrodynamics," Phys. Rev. Lett. **123**, 138002 (2019).

[71] S. Pradeep, A. Wessel, and L. C. Hsiao, "Hydrodynamic origin for the suspension viscoelasticity of rough colloids," J. Rheol. **66**, 895 (2022).

[72] B. J. Alder and T. E. Wainwright, "Phase transition for a hard sphere system," J. Chem. Phys. **27**, 1208 (1957).

[73] E. Lange, J. B. Caballero, A. M. Puertas, and M. Fuchs, "Comparison of structure and transport properties of concentrated hard and soft sphere fluids," J. Chem. Phys. **130**, 174903 (2009).

[74] P. C. Martin, O. Parodi, and P. S. Pershan, "Unified hydrodynamic theory for crystals, liquid crystals, and normal fluids," Phys. Rev. A **6**, 2401 (1972).

[75] J. Mewis and N. J. Wagner, *Colloidal Suspension Rheology* (Cambridge University Press, 2012).

[76] M. Fuchs, *Nonlinear Rheological Properties of Dense Colloidal Dispersions Close to a Glass Transition Under Steady Shear* (Springer, 2010).

[77] E. Zaccarelli, S. M. Liddle, and W. C. K. Poon, "On polydispersity and the hard sphere glass transition," Soft Matter **11**, 324 (2015).

[78] T. Sentjabrskaja, E. Zaccarelli, C. De Michele, F. Sciortino, P. Tartaglia, T. Voigtmann, S. Egelhaaf, and M. Laurati, "Anomalous dynamics of intruders in a crowded environment of mobile obstacles," Nat. Commun. **7**, 11133 (2016).

[79] T. Voigtmann and J. Horbach, "Double transition scenario for anomalous diffusion in glass-forming mixtures," Phys. Rev. Lett. **103**, 205901 (2009).